Iranian Journal of Geophysics, Vol 19 No 6, 2026, Page 139 – 150 (Research Article)
DOI: 10.30499/ijg.2025.474489.1626

Local earthquake tomography and 4-D imaging of the Rudbar Lorestan dam in Iran

Nasrin Pour Shabani[1], Hossein Shomali[2*] and Ahmad Sadidkhouy[3]

[1]*M.Sc., Institute of Geophysics, Department of seismology, University of Tehran, Tehran, Iran*
[2] *Professor, Institute of Geophysics, Department of seismology, University of Tehran, Tehran, Iran*
[3]*Associate Professor, Institute of Geophysics, Department of seismology, University of Tehran, Tehran, Iran*

(Received: 27 August 2024, Accepted: 18 February 2025)

Abstract

This study focuses on analyzing the crustal velocity structure at the Rudbar Dam located in Lorestan Province, using advanced earthquake tomography techniques. Local earthquake tomography is a powerful tool that provides crucial insights into various subsurface structures by generating a three-dimensional (3-D) velocity model of the region. Understanding crustal velocity structures and the anomalies that can arise within them is vital for improving our comprehension of fault geometries and other subsurface features, such as sediment layers, which are essential for regional seismic studies. By detecting these structural anomalies, we can significantly enhance our understanding of the area's tectonic behavior, contributing to better-informed assessments of seismic risks.

The research included data from 920 initial earthquakes, which were meticulously recorded by a network of seven short-period seismic stations strategically positioned around the dam. To calculate the crustal structure in this area, we utilized the SimulPS12 software, a robust tool designed for processing and analyzing seismic data to produce accurate velocity models.

Initially, we developed and presented a one-dimensional (1-D) velocity model, which serves as a foundational step in the analysis. Following this, we employed the Joint Hypocenter Determination (JHD) method to relocate the earthquakes more precisely, ensuring the accuracy of the subsequent three-dimensional (3-D) velocity model. The resulting 3-D velocity model images clearly depict the region's geological features, particularly highlighting the anticlines characterized by high-velocity cores and the synclines with low-velocity cores. These findings align well with the existing geological evidence, further validating the accuracy and reliability of our model.

The study also incorporates a four-dimensional (4-D) tomography approach to analyze temporal changes in the velocity structure. In this context, two distinct time windows were considered for data analysis: one prior to dewater and another after the injection process. This temporal analysis allowed us to observe significant changes in seismic activity, with the seismicity cluster shifting either towards the northwest or southeast following dewater. This movement suggests a correlation between the injection process and the observed seismicity patterns, offering insights into how human activities can influence seismic behavior.

By employing 4-D tomography, we concluded that fluctuations in pore pressure, induced by dewater, can have a substantial impact on the mechanical resistance of fault sections. This, in turn, influences seismic activity along the active faults in the region. These findings underscore the importance of monitoring subsurface pressure changes, as they can have direct implications for seismic hazard assessments, especially in regions with active fault systems like Lorestan.

Keywords: Local earthquake tomography, 3D and 4D velocity model, seismic images

[*]Corresponding author: shomali@ut.ac.ir

1 Introduction

In geologically intricate areas with difficult seismic reflection exploration, high-resolution local earthquake tomography (LET) is beneficial for the characterization of geothermal potential and hydrocarbon reservoirs (Calò and Dorbath, 2013; Zhang and Lin, 2014), as are the methods of fuzzy seismic inversion techniques (Jahanjooy et al., 2024) and simultaneous prestack inversion (Moghanloo et al., 2018) that improve the resolution of subsurface features like channels and reservoir facies. The aim of LET is to improve the estimation of the model parameters (velocity structure and hypocenters) by perturbing them in order to minimize the weighted root-mean-square (RMS) misfit (Thurber and Eberhart-Phillips, 1999). We have applied the linearized iterative Simulps12 inversion method which was developed originally by Thurber (1983) and improved by Eberhart-Phillips and Reyners (1997) to simultaneously determine 3-D V_p model and earthquake locations in a small region in south-west Iran. In this paper, we will present the inversion results for the upper crustal structure by 3-D seismic tomography which gives us significant comprehension of the important structures of the region. In the following, we will present 4-D tomography which has emerged as promising a new method in the field of seismology. This approach includes the integration of 3-D tomographic images with time-lapse data, like seismic waves recorded over a period of time (Gunasekera et al.,2003). By integrating these types of data, researchers can obtain insights into the dynamic processes occurring within the earth. The use of 4-D tomography provides to study changes in elastic properties that happen during the resurgence of seismic congestion. By applying this approach, we will gain a better understanding of how earthquakes are triggered and how geological structures in the Earth's crust respond to stress and strain. Ultimately, this approach can help us to mitigate the risks associated with induced seismicity, particularly in areas where human activities such as oil and gas exploration or geothermal energy production may trigger seismic events.

2 Geological and Seismotectonic

The area is restricted to 50 * 50 km^2 where is in in the western part of Iran from 32.75 to 33.25 9 (latitude) to 49.50 to 50 (longitude); also, the Rudbar dam is located in the Zagros Mountain range in the west of Iran (Najafabadi, 2013). The location of the dam is in narrow gates with steep walls made of dolomitic limestones of the Dalan formation. Hormuz Formation is the oldest outcrop formation around the Rudbar Dam of Lorestan (Najafabadi, 2013). In this area, the rocks are mainly limestone, dolomite, shale, and marl. The highest points are the ridges of the Dalan formation located near the Chal Hatem and arranged in northwest-southeast strips (Hydrogeology Report, 2006). The outcrops of the Dalan formation is 350 to 400 m thick and are made of limestone and dolomitic limestone where is located around the Rudbar Dam (Lorestan Rudbar dam engineering geological report, 2006). The most direction of the faults in the study area is northwest-southeast and their function are mainly strike-slip, and some are reversed. According to Kerami and Azizi (2014), hidden anticlines and faults with reverse mechanisms are in the vicinity of Rudbar Dam.

3 Data and Method

In this study, we have used P-waves arrival times that were recorded by a local

seismic network operated by the Parsian Company between 2014 to 2018. Signal processing consist of removing low-quality records from the data. To do this, we have used the conditions identified in Table 1.

Table 1. Conditions of the high-quality data selection.

Min. P phase	4	Max. RMS	0.2 (s)
Max.Horizontal errors	3.0 (km)	Max.Vertical errors	1.5 (km)

This study has used the 1-D velocity model of Yamini Fard et al (2006) by averaging Vp between the layers for the upper part of the crust, and for the lower crust we have used the iasp91 model (Kennett, 1991; Fig. 1). By using the criteria listed in Table 1, the number of earthquakes decreased from about 920 to 660 (Fig 2), resulting in a final dataset with 2790 P-phases observations.

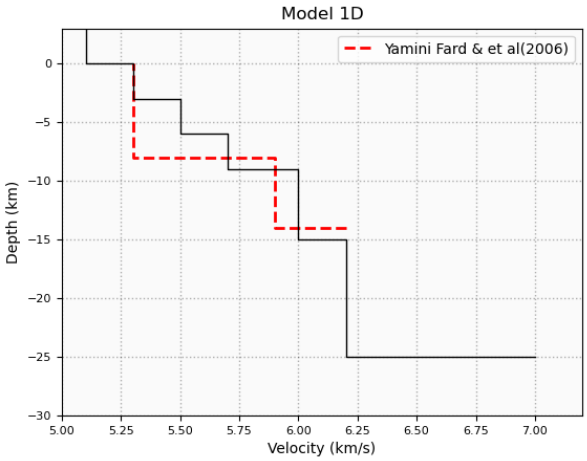

Figure 1. The 1-D velocity model of Yamini Fard et al. (2006) is marked with a red dashed line, and the black line is the 1-D velocity model presented in the study.

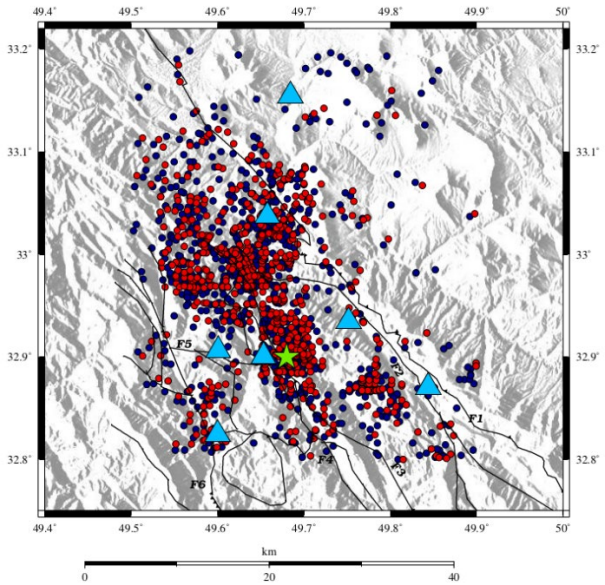

Figure 2. The initial data is in blue and the data after relocation is in red. The blue triangles are the locations of the stations, and the green star shows the location of the dam.

The Joint Hypocenter Determination (JHD; Douglas, 1967) method has been used to improve the location of earthquakes. This method is used to relocate a group of earthquakes together, is generally more precise than the single event method, and it is less affected by the choice of velocity structure model, as noted by Pujol (1995), Pujol et al. (1997), and Quintero and Kissling (2001). The locations of seismic stations and epicenters of relocated earthquakes are shown in Figure 3.

We have used a damped least-squared iterative (Thurber, 1983; Evans et al., 1994) to dissolve the non-linear tomography problem (Haslinger and Kissling, 2001; Husen et al., 2003). This method entailed performing iterative damped least squares inversions to concurrently derive earthquake locations and velocity model parameters. Hypocenter locations are included in the inversion as unknowns, due to the coupling of hypocenter locations and velocities (Thurber, 1992). Furthermore, we have utilized full 3-D shooting ray tracing (Haslinger and Kissling, 2001) to compute travel times through the velocity model.

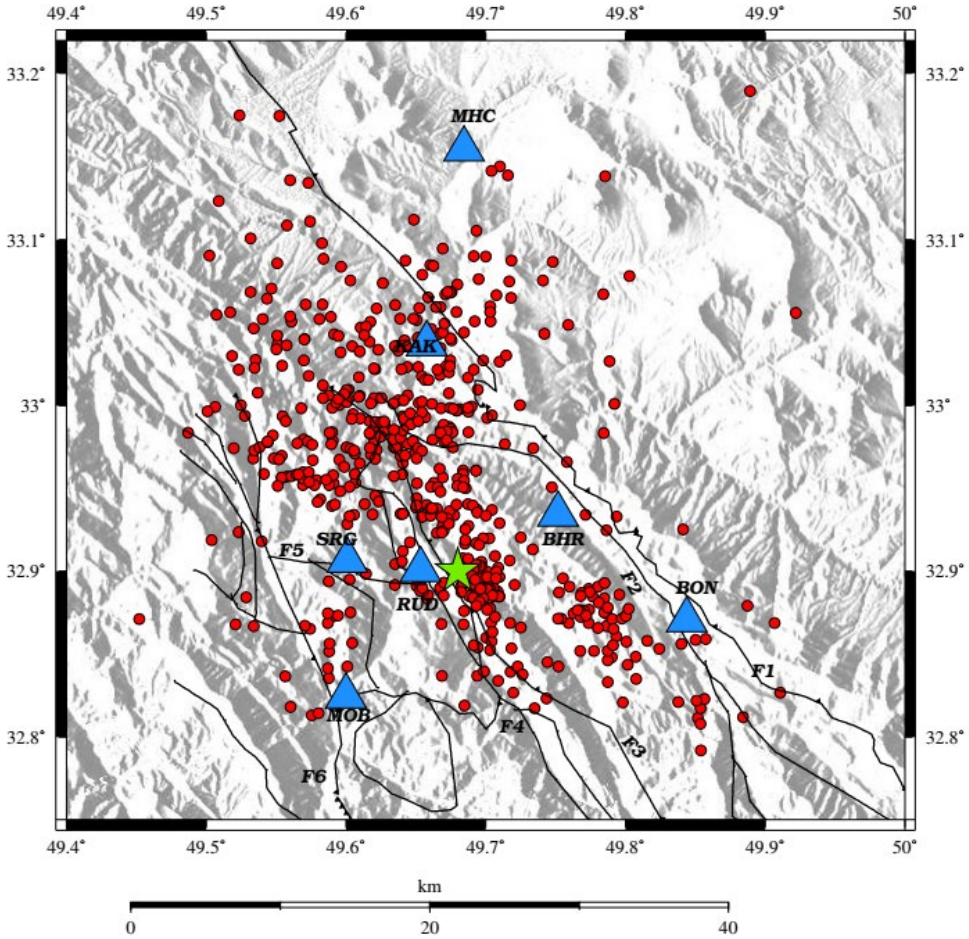

Figure 3. The locations of earthquakes after the inversion. The blue triangles are the locations of the stations, and the green star shows the location of the dam.

Damping parameters have been chosen empirically by evaluating the trade-off between data and solution variance, as suggested by Eberhart-Phillips (1986), the chosen value is 50 for the V_p model (Fig. 4). The value of input and output RMS for the inversion step was 0.071(s) and 0.028(s), respectively. After the inversion process, the RMS of the total earthquakes were decreased by 60% compared to the initial state of the earthquakes.

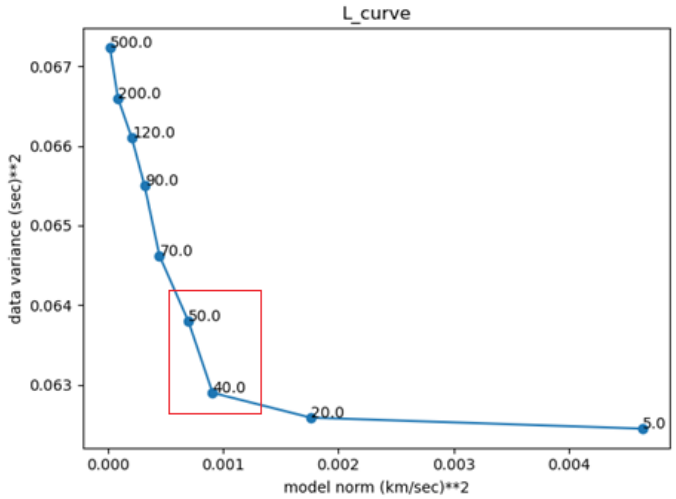

Figure 4. After three iterations, a trade-off curve that depicts the relationship between data variance and model variance (Eberhart-Phillips, 1986) in each solution. Two values of 40 and 50 are suitable for damping, but after doing an inversion, the value of 50 had significant effects in improving the results.

5 3-D V_p model description

A significant problem in seismic tomography is optimizing and evaluating the spatial resolution of the estimated model. Model resolution is limited by various factors including data errors and the 3-D geometry of the crossing-rays through the volume, to evaluate the resolution of the dataset, we have used DWS test (Fig. 5). The results of local earthquake tomography using the P-wave travel time method in the studied area indicate the presence of significant velocity anomalies up to 6 km deep in the upper crust, and the results are shown in Figure 5. The station MHC has the lowest resolution at different depths and no resolution at a depth of 9 km.

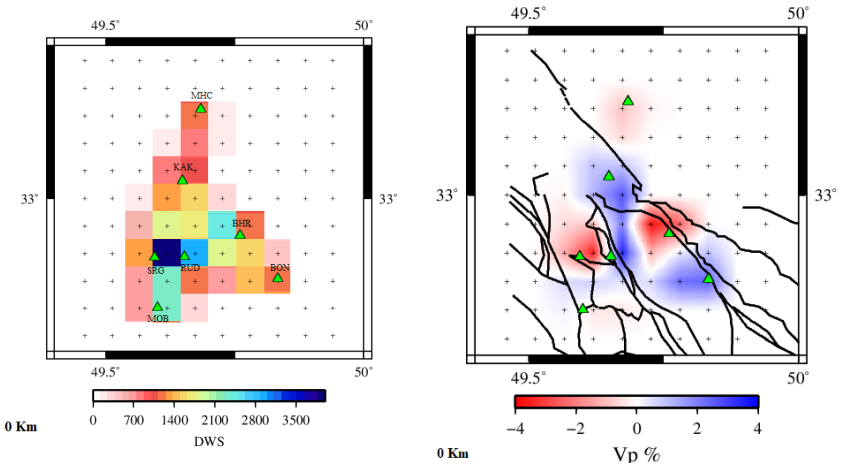

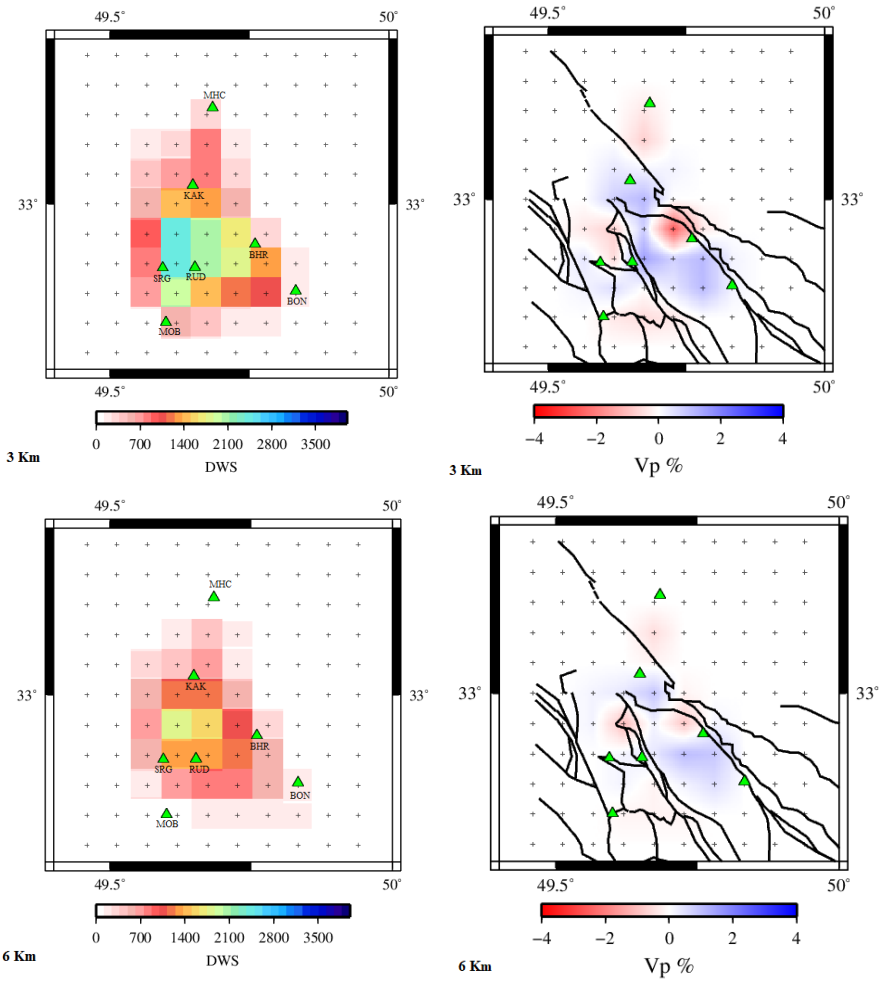

Figure 5. Two distinct layers are shown at depths 3 and 6 km, each with corresponding DWS parameters and P-wave velocity (Vp) values. On the right-hand side of the figure, the P-wave velocity (Vp) profile is displayed, ranging from +4 km/s to -4 km/s, and extending to a depth of 6 kilometers. Regarding the DWS parameter, lower values are indicative of reduced model resolution, suggesting a decreased ability to resolve finer structural details at those depths. The seismic stations in the region are marked by green triangles.

In Figure 6a, section A-A^ and section B-B^ with 20 km and 28 km length from the southwest to the northeast passes through from Dam, respectively. The width of each drawn section is equal to 10 km and the slope of them is set to 90 degrees. A-A^ section begins with a positive anomaly; then, the anomaly value changes to a negative value, and positive anomaly is seen under the Rudbar Dam. B-B^ section starts with a negative anomaly, and in the middle of the section, the anomaly changes to a positive value and continues to nearly 9 km in depth (Fig 6b).

Beneath the Dam, earthquakes had occurred at depths close to the surface, and high-velocity anomalies can be seen in this area. According to the geological evidence, the high-speed parts of this section are related to the Mila Formation, which is composed of limestone and shale. Between the F1 (MZRF fault) and F2 faults, earthquakes have occurred at greater depths, and anomalies can be seen up to a depth of nearly 5 km. As

shown in the figure, the low-velocity and high-velocity parts correspond to syncline and anticline, respectively, which is consistent with the geological findings of the area and with Kerami and Azizi (2014) studies.

6 Repeated Time Tomography (4-D)

In order to reduce the seismic risk in highly vulnerable areas, the 4-D tomography travel time method is currently used in areas such as volcanic, tectonic, etc., using passive seismic sources (Londoño and Kumagai, 2018). Also in recent years, many studies have been carried out in seismically active zones using 4-D tomography (e.g., Valoroso et al. 2011, Vargas et al. 2017, Abacha et al. 2023). It should be emphasized that in most geological processes even the smallest changes that occur may not be detectable by repeated tomographic reversals. In fact, such inversions do not always allow one to distinguish the actual deviations from the artifacts resulting from the variations in the data range. Therefore, it is important to approach geological process analysis with caution and to consider the limitations of available tools and methods (Koulakov et al., 2018).

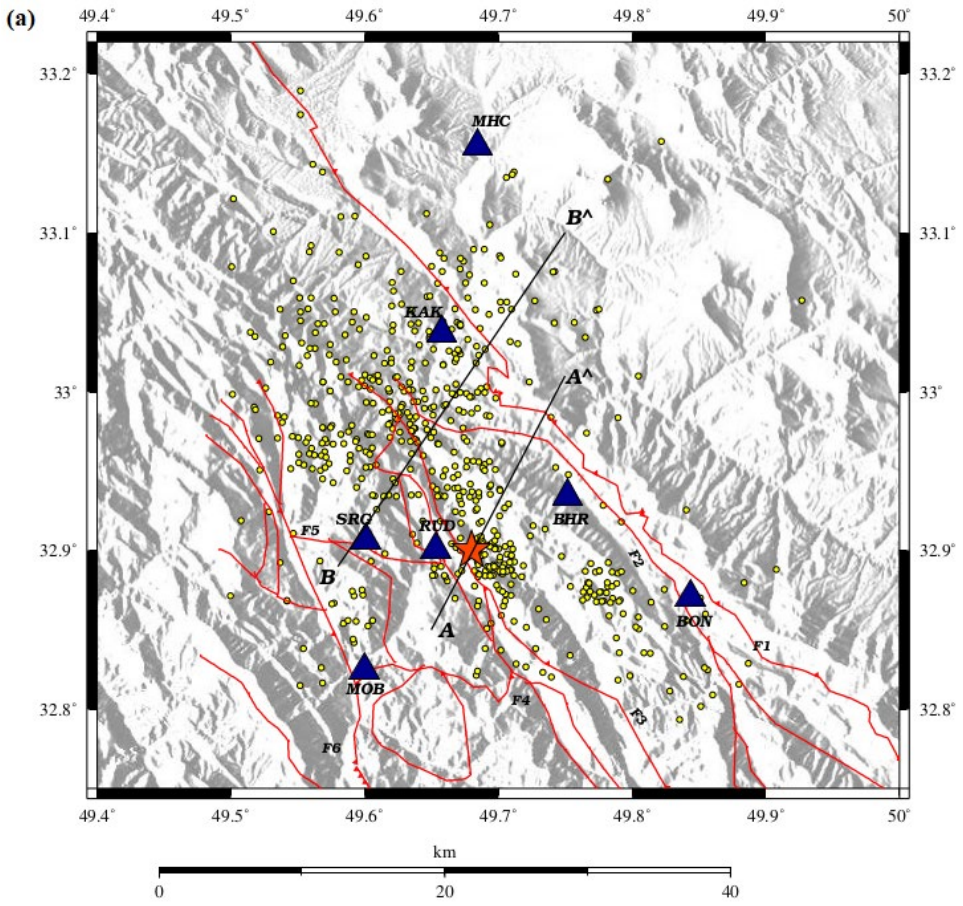

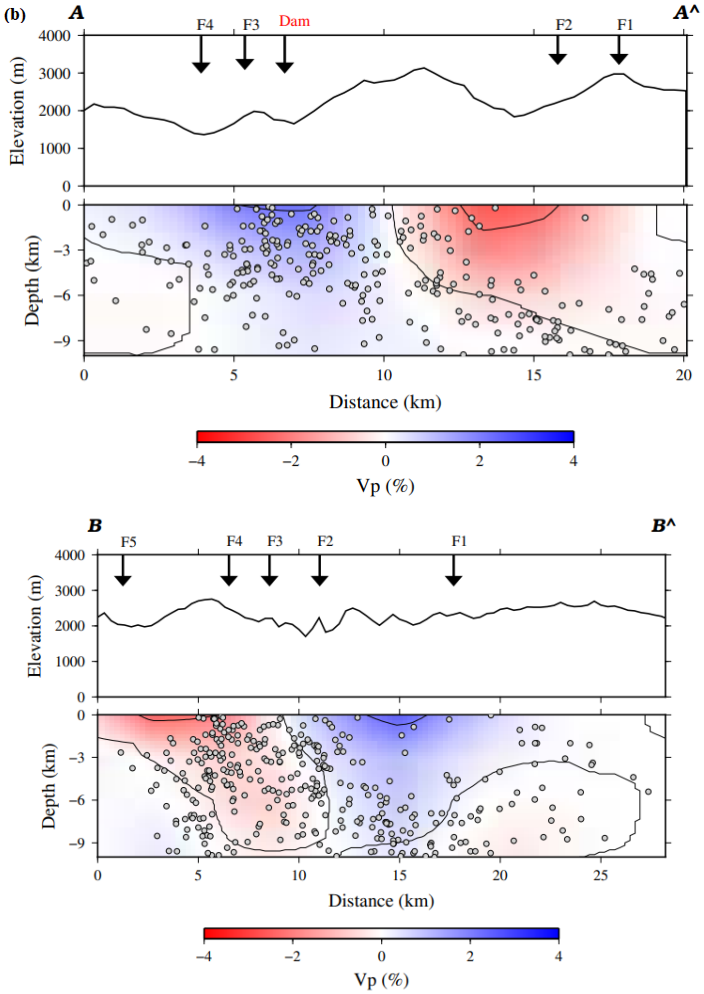

Figure 6. (a) The position of the vertical cross sections. (b) Vertical cross sections of the final three-dimensional velocity model obtained from P-wave tomography based on the percentage of P-wave velocity changes compared to the initial velocity in the studied area.

The 4-D tomography is very challenging because it needs to time-windows of the same length, and the number of rays passing through an area must be the same for the time-windows considered. In this study, we have investigated the ability of 4-D tomography P-wave seismic to provide images of the volume containing the reservoir in order to identify and track the pore pressure disturbance caused by the increase in water in the dam. To perform 4-D tomography, the same 1-D velocity model and optimized parameters are used in the 3-D inversion. To perform 4-D tomography, the same 1-D velocity model and optimized parameters are used in the 3-D inversion. We have divided the data into two time-windows, the Epoch A time-window corresponds to before dewatering, and the Epoch B time-window corresponds to after dewatering (Fig 7).

In this part, after determining the length of the two time-windows, the earthquakes in both Epochs have relocated, and the inversion stage have implemented. The number of earthquakes in both windows are approximately 300 events. In each Epoch, the location of earthquakes before and after the dewater are shown in yellow and gray colors, respectively (Fig 8).

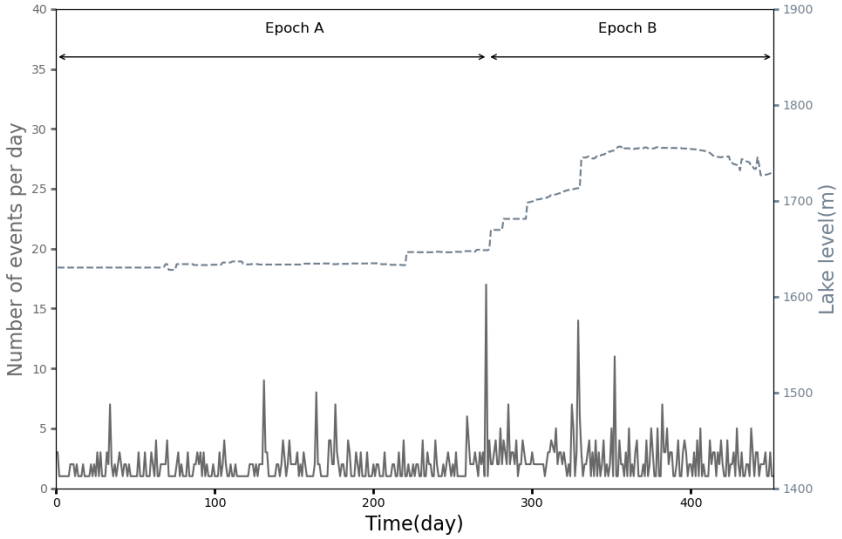

Figure 7. Seismicity curve with time; the gray line is the number of events per day; the dashed gray line is the level of lake water.

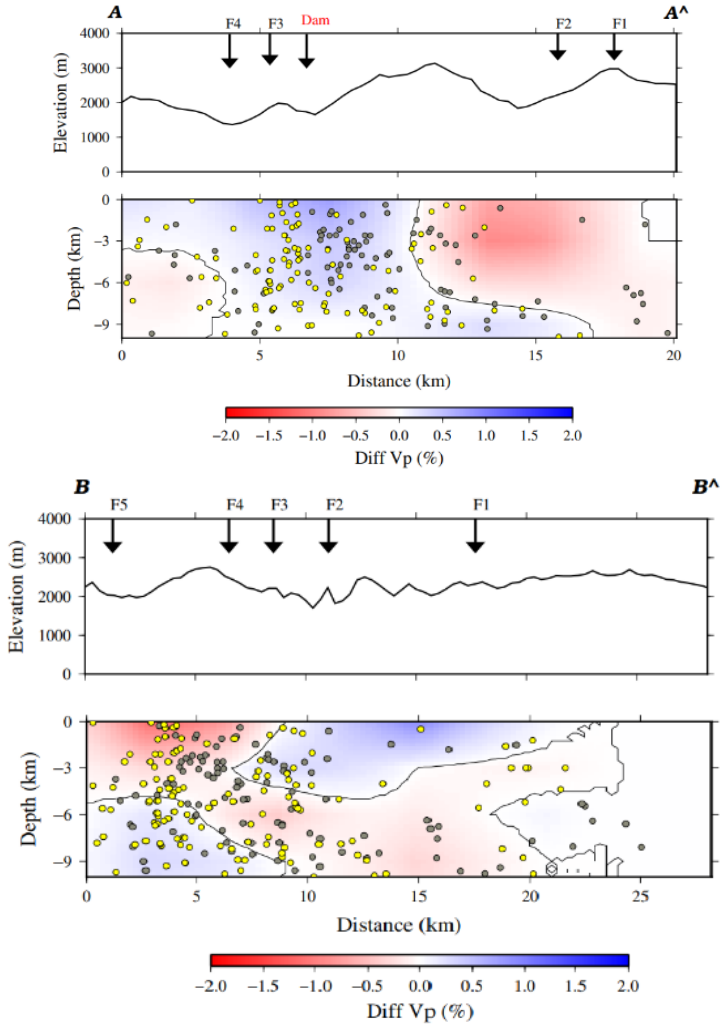

Figure 8. Vertical cross sections showing ΔV_P model between the two epochs (Epoch B – Epoch A). Yellow circles represent Epoch A window's earthquakes and gray circles represent Epoch B window's earthquakes.

7 Conclusion

The RMS values for the input and output of the inversion step were 0.071 s and 0.028 s, respectively, which shows that the RMS of the total earthquakes after inversion has a 60% reduction compared to the initial state. Also, 84% of the earthquakes have an RMS of less than 0.1 s after performing the JHD method, and 90% of the earthquakes have an RMS of less than 0.05 s after performing the inversion process. This indicates a substantial improvement in the accuracy of earthquake locations. The anticline and syncline observed in the sections (Fig 6b, anticline and syncline with high and low velocity, respectively) are consistent with the geological findings, Kerami and Azizi (2014).

In the 4-D tomography, before the dewater, a number of earthquakes occurred nearly the dam and in the south of the area, and the dewater caused earthquakes occurred in the eastern part of the area at greater depths. Before the dewater, the earthquakes were located vertically under the dam construction (Fig 8), after the dewater, the earthquakes have moved in the northwest direction (they have moved towards the F1 and F2 faults, which are among the seismic and active faults in the region). This made us realize that pore pressure fluctuations can affect the resistance of fault sections and support seismic changes along active faults.

Acknowledgment

All data used in this study was collected and disseminated by the Parsian Seismic Network. We would like to express our gratitude to Mrs. Sabouri and Mr. Masih for their assistance in data collection, and to Dr. Rahim Jomiri for his expertise in data processing. We also extend our heartfelt thanks to the anonymous reviewers for their insightful feedback and constructive comments, which significantly contributed to enhancing the quality of this work.

References

Abacha, I., Bendjama, H., Boulahia, O., Yelles-Chaouche, A., Roubeche, K., Rahmani, S. T. E., ... & Tikhamarine, E. M. (2023). Fluid-driven processes triggering the 2010 Beni-Ilmane earthquake sequence (Algeria): evidence from local earthquake tomography and 4D Vp/Vs models. *Journal of Seismology*, *27*(1), 77-94.

Calò, M., & Dorbath, C. (2013). Different behaviours of the seismic velocity field at Soultz-sous-Forêts revealed by 4-D seismic tomography: case study of GPK3 and GPK2 injection tests. Geophysical Journal International, 194(2), 1119-1137.

Douglas, A. (1967). Joint epicentre determination. *Nature*, *215*(5096), 47-48.

Eberhart-Phillips, D. (1986). Three-dimensional velocity structure in northern California Coast Ranges from inversion of local earthquake arrival times. Bulletin of the Seismological Society of America, 76(4), 1025-1052.

Eberhart-Phillips, D., & Reyners, M. (1997). Continental subduction and three-dimensional crustal structure: The northern South Island, New Zealand. Journal of Geophysical Research: Solid Earth, 102(B6), 11843-11861.

Engineering Geological Report of the Second Phase of the Lorestan Rudbar Dam and Power Plant Project, (2006). Quds Niro Consulting Engineers.

Evans, J. R., Eberhart-Phillips, D., & Thurber, C. H. (1994). User's manual for SIMULPS12 for imaging Vp and Vp/Vs; a derivative of the" Thurber"

tomographic inversion SIMUL3 for local earthquakes and explosions (No. 94-431). US Geological Survey.

Gunasekera, R. C., Foulger, G. R., & Julian, B. R. (2003). Reservoir depletion at The Geysers geothermal area, California, shown by four-dimensional seismic tomography. Journal of Geophysical Research: Solid Earth, 108(B3).

Haslinger, F., & Kissling, E. (2001). Investigating effects of 3-D ray tracing methods in local earthquake tomography. Physics of the Earth and Planetary Interiors, 123(2-4), 103-114.

Husen, S., E. Kissling, N. Deichmann, S. Wiemer, D. Giardini, and M. Baer (2003), Probabilistic earthquake location in complex three-dimensional velocity models: Application to Switzerland, J. Geophys. Res., 108, doi: 10.1029/2002JB001778.

Hydrogeological report, (2006). studies of the identification phase of the long tunnel for Anuj water transmission to Qamroud, Mahab Quds Company.

Jahanjooy, S., Hashemi, H., & Bagheri, M. (2024). Fuzzy Seismic Inversion: A Case Study on Channel Features in Johnson Formation of Browse Basin, Australia. Journal of the Earth and Space Physics, 49(4), 93-104.

Karmi, J., Azizi, A., (2014). Investigating the reasons for changing the Lorestan River Dam option from RCC to ECRD in terms of tectonics and seismicity, National Conference of Civil Engineering and Geology, Aliguderz, https://civilica.com/doc/590215

Kazemi Najafabadi, A. (2013). engineering geology of the part of the pump-storage system of the Rudbar dam and power plant of Lorestan, National Conference of Geology and Resource Exploration, Shiraz, https://civilica.com/doc/373736/

Kennet, B. L. N. (1991). IASPEI 1991 seismological tables. Terra Nova, 3(2), 122-122.

Koulakov, I., Smirnov, S. Z., Gladkov, V., Kasatkina, E., West, M., El Khrepy, S., & Al-Arifi, N. (2018). Causes of volcanic unrest at Mt. Spurr in 2004–2005 inferred from repeated tomography. Scientific reports, 8(1), 17482.

Londoño, J. M., & Kumagai, H. (2018). 4D seismic tomography of Nevado del Ruiz Volcano, Colombia, 2000–2016. Journal of Volcanology and Geothermal Research, 358, 105-123.

Moghanloo, H. G., Riahi, M. A., & Bagheri, M. (2018). Application of simultaneous prestack inversion in reservoir facies identification. Journal of Geophysics and Engineering, 15(4), 1376-1388.

Pujol, J. (1995). Application of the JHD technique to the Loma Prieta, California, main shockaftershock sequence and implications for earthquake location: Bulletin of the Seismological Society of America, 85, 129– 150.

Pujol, J., Johnston, A. Chiu, J. M., and Yang, Y. T. (1997). Refinement of thrust faulting models for the central New Madrid seismic zone: Engineering Geology, 46, 281–298.

Quintero, R., and Kissling, E., (2001). An improved P-wave velocity reference model for Costa Rica: Geofísica Internacional, 40(1), 3-19.

Thurber, C.H., (1983). Earthquake locations and three-dimensional crustal structure in the Coyote Lake area, central California. J. Geophys. Res. 88, 8226–823

Thurber, C. H. (1992). Hypocenter-velocity structure coupling in local earthquake tomography. Physics of

the Earth and Planetary Interiors, 75(1-3), 55-62.

Thurber, C., & Eberhart-Phillips, D. (1999). Local earthquake tomography with flexible gridding. Computers & Geosciences, 25(7), 809-818.

Vargas, C., Koulakov, I., Jaupart, C., Gladkov, V., Gomez, E., El Khrepy, S., & Al-Arifi, N. (2017). Breathing of the Nevado del Ruiz volcano reservoir, Colombia, inferred from repeated seismic tomography. Scientific Reports, 7(1), 1-6.

Valoroso, L., Improta, L., De Gori, P., & Chiarabba, C. (2011). Upper crustal structure, seismicity and pore pressure variations in an extensional seismic belt through 3-D and 4-D VP and VP/VS models: The example of the Val d'Agri area (southern Italy). Journal of Geophysical Research: Solid Earth, 116(B7).

Yamini-Fard, F., Hatzfeld, D., Tatar, M., & Mokhtari, M. (2006). Microearthquake seismicity at the intersection between the Kazerun fault and the Main Recent Fault (Zagros, Iran). Geophysical Journal International, 166(1), 186-196.

Zhang, Q., & Lin, G. (2014). Three-dimensional Vp and Vp/Vs models in the Coso geothermal area, California: Seismic characterization of the magmatic system. Journal of Geophysical Research: Solid Earth, 119(6), 4907-4922.